Supporting Information: Role of Dynamically Frustrated Bond Disorder in a Li^+ Superionic Solid Electrolyte

Nicole Adelstein*,†,‡ and Brandon C. Wood*,†

†*Materials Science Division, Lawrence Livermore National Laboratory, Livermore, CA 94550, USA*

‡*Current address: Department of Chemistry and Biochemistry, San Francisco State University, San Francisco, CA 94132, USA*

E-mail: nicoleal@sfsu.edu; brandonwood@llnl.gov

Additional calculation details

The first-principles molecular dynamics calculations were performed using the following pseudopotentials from the Quantum ESPRESSO website: Li.pbe-s-van_ak.UPF, In.pbe-d-rrkus.UPF, and Br.pbe-van_mit.UPF. The theoretically optimized lattice vectors for the supercell were $\mathbf{a} = \mathbf{b} = 13.4411$ Å, $\mathbf{c} = 25.7397$ Å, and $\gamma = 109.3°$.

Maximally Localized Wannier Functions "MLWF" were constructed using the Wannier90 code. The converged electron density was taken from each frame as an input. The wavefuctions were initialized by projecting the electron density onto an s orbital for Li, an sp^3 orbital for Br and d orbitals for In. The projection was considered maximally localized if the change in the spread between iterations was less than 1×10^{-6} Å^2.

In Fig. 2 of the main text, the Wannier centers (WCs) on Br^- are assigned to Li^+, In^{3+}, or neither (free) via the following algorithm. For each cation, the six nearest neighbor Br^-

anions are determined and then the closest WC, on each Br^-, to the cation is designated. These six WCs are considered associated with that cation. Note that this algorithm permits WCs to be shared between two cations and also allows for WCs to be associated with no cations at all. The latter case is given the designation "free". When WCs are shared between two cations, only the cation with the most direct WC alignment (smallest Li–Br–WC angle) is included in the analysis of Fig. 2.

The algorithm to distinguish jumping Li^+ from ordinary Li^+ is as follows. The index of the six nearest Br^- neighbors to each Li^+ is recorded. When Li^+ jumps into a neighboring octahedral site through the tetrahedral site, it will share two out of six neighbors with the previous octahedral site. When Li^+ is rattling around in the octahedral site, it will often move far enough to retain only four of six Br^- neighbors. Thus, a jumping Li^+ is defined as having changed three or more Br^- neighbors, which controls for the above possibilities. The initial jump frame is recorded when three Br^- neighbors change, and the jump ceases when four Br^- neighbors change and the neighbor list becomes static. All frames that have at least three switched Br^- neighbors over the jump time interval are therefore associated with the jumping Li^+, which encompasses Li^+ occupation in the tetrahedral site as well as transition states between octahedral and tetrahedral sites. The length of a jump is constrained to be under 400 fs, since recording changes in neighbors that occur over longer time periods often picks up multiple jumps.

The algorithm for formation or breaking of a polar-covalent bond includes a hysteresis function that limits fictitious bond fluctuations at short timescales near the transition state. The primary cutoffs for angle and distance taken from Fig. 3 are $\theta = 23°$ and $R = 3.15$ Å, respectively. However, for angles in the $21 - 25°$ range, where fluctuations between bound and unbound states are highest, we instead retain the memory of the previous bonding state. Therefore, θ must decrease below 21° for a polar-covalent bond to break and increase above 25° for a new polar-covalent bond to form.

The times associated with bond-breaking events were recorded for each Li^+ ion according

to the above algorithm to generate a spectrum with $h(t) = 1$ if a bond breaks and $h(t) = 0$ otherwise. The corresponding frequency for collective bond breaking of all Li^+ was computed according to $f(\omega) = \tilde{F}\left[\sum_i h(t)\right]$, where $\tilde{F}$ represents the Fourier transform and the sum runs over all N Li^+ ions in the supercell. The frequency for individual bond breaking was computed according to $f(\omega) = \frac{1}{N}\sum_i \tilde{F}\left[h(t)\right]$.

Supporting data

To obtain additional physical insight into the relative degree of the covalency at the octahedral site and during Li^+ jumping, we selected a pathway for Li^+ migration derived from a nudged elastic band (NEB) calculation and extracted representative local-minimum octahedral and tetrahedral configurations. Projected electronic densities of states (pDOS) were computed for jumping Li^+ and for the two Br^- ions that remained coordinated in polar-covalent bonds throughout the octahedral-to-tetrahedral transition. The results, shown in Fig. S1 (a), demonstrate a higher degree of Li-Br hybridization at the tetrahedral site than at the octahedral site, as expected from the MLWF analysis (note that the PDOS analysis does not account for multipole moment contributions that likely also contribute). Br 1 has three Li neighbors and Br 2 has two Li neighbors and 1 In neighbor.

The pDOS differences (ΔpDOS) in Fig. S1(b) and (c) are taken between each polar-covalent Br^- and the scaled average of its Li^+ neighbors. As the jumping Li^+ passes through the tetrahedral site, the overlap (covalent bonding) with ALL Li^+ neighbors increases, such that ΔpDOS decreases (red) compared to when Li^+ is in the octahedral site (black).

The increased hybridization of the tetrahedral site affects the site energies and landscape. To see this more clearly, we ran a new series of static calculations in which we replaced a "host" Br^- with Cl^- or I-. According to Fajan's rules, substitution with Cl^- should weaken the covalent character, whereas substitution with I- should strengthen it. In this way, we sought to tune the covalent contribution within a more controlled computational environment, although these calculations neglect the complex interplay and dynamical correlations

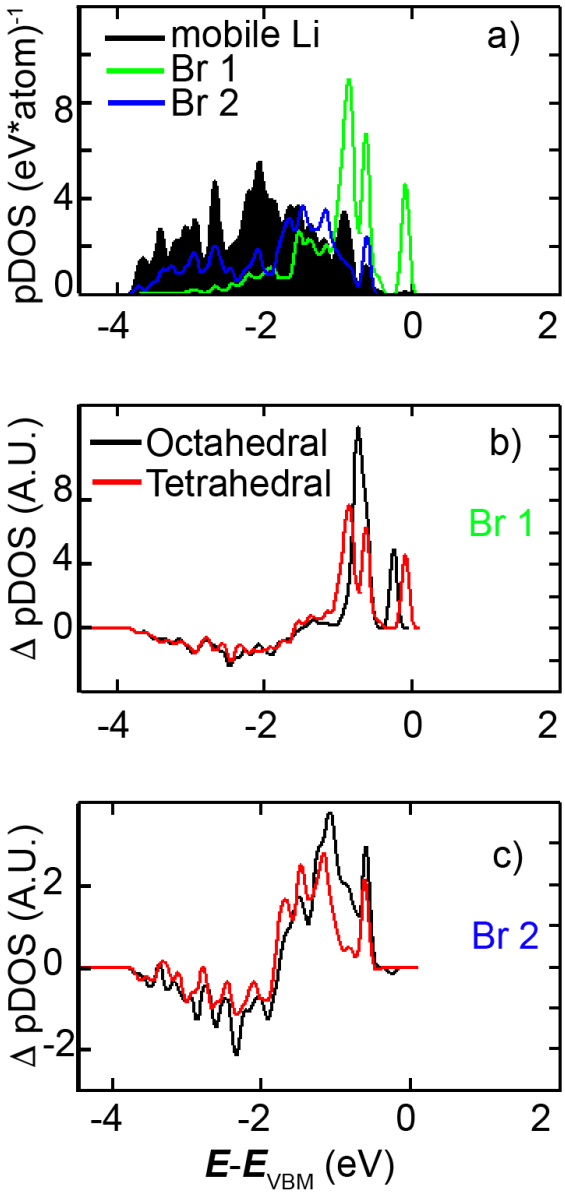

Figure S1: Valence projected electronic densities of states for Li–Br polar-covalent bonds during an octahedral-to-tetrahedral Li^+ migration. (a) pDOS of mobile Li^+ and two Br^- ions forming polar-covalent bonds in the tetrahedral site. (b) and (c) show the difference in pDOS for the two Br^- ions with respect to Li^+ in both the octahedral and tetrahedral sites. Energies are referenced to the valence band maximum.

afforded by our dynamics analysis.

Substituting the "host" Br- anion for Cl^- and I^- gave the charge density differences shown in Fig. S2, from which the directionality of the Li-anion interactions becomes visible. The magnitude of the distortions, which bear remarkable resemblance to the MLWF description, follows the order expected from Fajan's Rules ($I^- > Br^- > Cl^-$). The presence of higher-covalency interactions between Li^+ and Br^-/I^- alters the charge distribution even along directions that lack any bound Li^+ (panels (b) and (d) in Fig. S2). Note also that the electron density does not increase uniformly in a sphere upon substitution of large anions, as would be expected for purely ionic bonding.

Based on this simple site model, we allowed the Li^+ position to relax to extract preferred Li-anion distances upon Cl^- or I^- substitution of the anion that "hosts" the migrating Li^+ during a jump event. Compared to energies, which are difficult to decompose into individual anion-cation contributions, these distances can be unambiguously compared and assigned. Fig. S3 shows the distances between the cation and host anion (d) in the octahedral and tetrahedral sites, compared with bond lengths expected from summing the cation and anion ionic radii ($r^+ + r^-$). Note that using the ionic radius reference allows for an unbiased comparison of Li-anion bonds that is independent of ion size (the bonds are shorter than the ionic radii predict, which is typical for crystalline ionic salts).

In the octahedral sites (black curve in Fig. S3), Cl^- forms the shortest bonds and I^- forms the longest bonds after correcting for the ion sizes. This qualitative trend can be rationalized by considering the anion electronegativity differences: single-site substitution with Cl^- will tend to draw Li^+ away from the other Br^- anions, resulting in a shorter bond length compared to that predicted by the ionic radii; this effect is weakened upon I^- substitution, since I^- is less electronegative than Br^-. By contrast, in the tetrahedral sites (red curve), I^- attracts Li^+ much more strongly than Cl^-. As discussed in the main text, the opposing trends between the octahedral and tetrahedral sites support the notion that the tetrahedral site has higher covalent character, and that jumping Li^+ cations experience

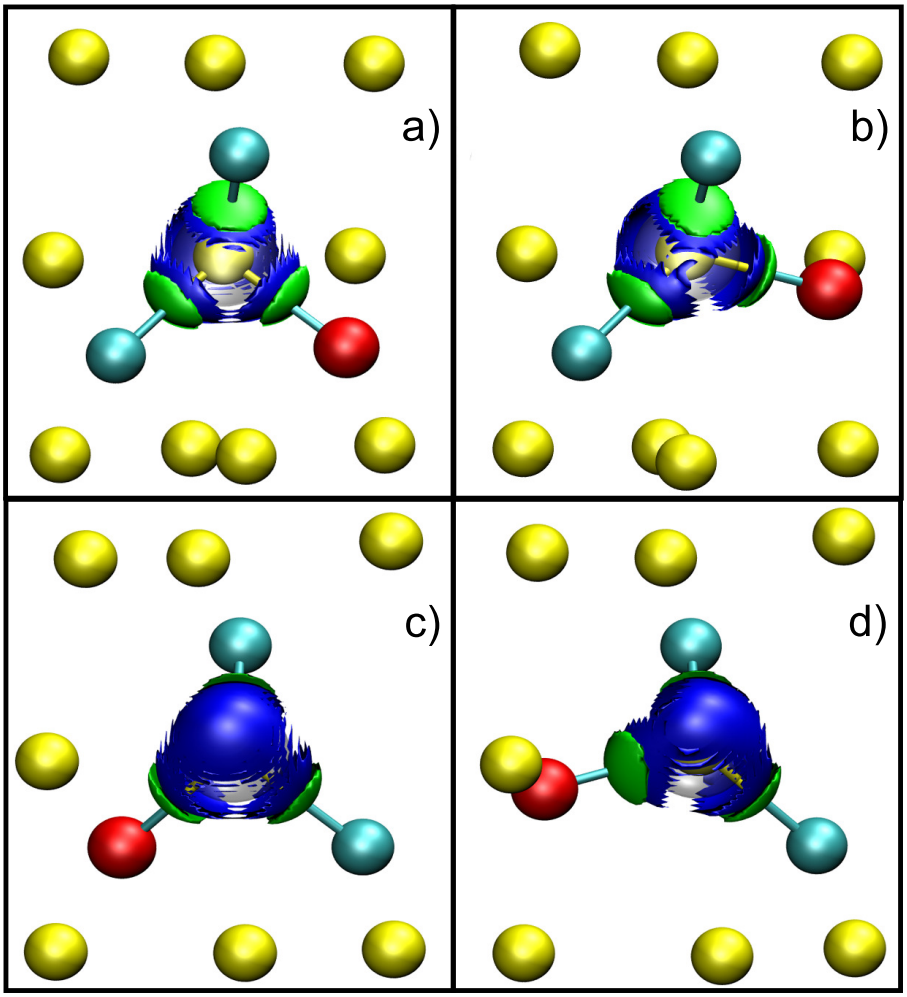

Figure S2: Electronic charge density differences ($\Delta\rho$) incurred upon substitution of one Br^- anion with I^- or Cl^- during a Li^+ jump from the octahedral site (panels (a) and (c)) via the tetrahedral site (panels (b) and (d)). In each case, three Li-anion polar-covalent bonds are formed. The Br^- anion that hosts the mobile Li^+ during the jump was selected for substitution. $\Delta\rho = \rho(I^-) - \rho(Br^-)$ is shown in green and $\Delta\rho = \rho(Br^-) - \rho(Cl^-)$ is shown in blue. Atomic positions were fixed to the geometry of the Br^-. The transparent gray sphere indicates where the electron density is taken from. The mobile Li^+ is red, the other Li^+ are cyan, and the anions are yellow. Panels (a) and (c) (or (b) and (d)) show the same density differences along two opposing directions. Note that the perturbation of the electronic density follows the anion-Li^+ bond direction. In panels (b) and (d), the site extending out of the page is vacant, yet the blue isosurface still shows a distortion towards the vacant site.

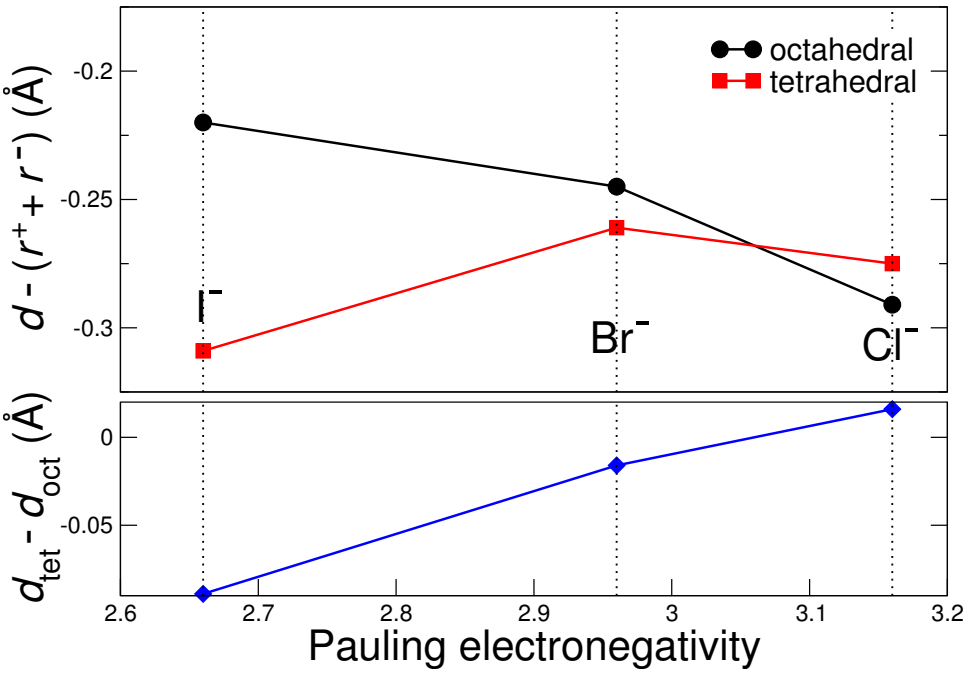

Figure S3: Lithium-anion bond distance d in the octahedral (black) and tetrahedral (red) sites for a local environment comprised exclusively of Br^-, compared to single-site substitution of I^- or Cl^-. Values are plotted against the electronegativity of the anion. Anion coordinates are fixed to the relaxed geometry of the unsubstituted lattice, whereas the cation is allowed to relax freely. Distances are compared to the value expected from a sum of the corresponding ionic radii ($r^+ + r^-$). The bottom panel shows the difference between the bond distances for the tetrahedral (d_{tet}) and octahedral (d_{oct}) sites; the upward trend can be interpreted as higher covalent character in the tetrahedral site.

fluctuating levels of covalent interaction as they migrate.

At higher temperature, the strength of the polar-covalent bond is generally weakened. Table S1 shows the breakdown of different types of WCs and bond types as a function of temperature, which confirms this point. The data are taken from an analysis of Figs. 8b–8d in the main text.

Table S1: Breakdown of bond types as a function of temperature, based on an analysis of Figs. 8b–8d.

Temperature	Free WC	Unbound Li	Bound Li	Indium
500 K	9.2%	29.0%	36.8%	25%
700 K	9.8%	29.2%	36.0%	25%
900 K	12.2%	30.3%	32.5%	25%